Nuclear Instruments and Methods in Physics Research A 743 (2014) 79–85

Contents lists available at ScienceDirect

Nuclear Instruments and Methods in Physics Research A

journal homepage: www.elsevier.com/locate/nima

Measurement of the angular distribution of fission fragments using a PPAC assembly at CERN n_TOF

D. Tarrío [a,*], L.S. Leong [b], L. Audouin [b], I. Duran [a], C. Paradela [a], L. Tassan-Got [b], C. Le Naour [b], C.O. Bacri [b], V. Petitbon [b], J. Mottier [b], M. Caamaño [a], S. Altstadt [c], J. Andrzejewski [d], M. Barbagallo [e], V. Bécares [f], F. Bečvář [g], F. Belloni [h], E. Berthoumieux [h,i], J. Billowes [j], V. Boccone [i], D. Bosnar [k], M. Brugger [i], M. Calviani [i], F. Calviño [l], D. Cano-Ott [f], C. Carrapiço [m], F. Cerutti [i], E. Chiaveri [h,i], M. Chin [i], N. Colonna [e], G. Cortés [l], M.A. Cortés-Giraldo [n], M. Diakaki [o], C. Domingo-Pardo [p], N. Dzysiuk [q], C. Eleftheriadis [r], A. Ferrari [i], K. Fraval [h], S. Ganesan [s], A.R. García [f], G. Giubrone [p], M.B. Gómez-Hornillos [l], I.F. Gonçalves [m], E. González-Romero [f], E. Griesmayer [t], C. Guerrero [i], F. Gunsing [h], P. Gurusamy [s], D. G. Jenkins [u], E. Jericha [t], Y. Kadi [i], F. Käppeler [v], D. Karadimos [o], P. Koehler [w], M. Kokkoris [o], M. Krtička [g], J. Kroll [g], C. Langer [c], C. Lederer [c,x], H. Leeb [t], R. Losito [i], A. Manousos [r], J. Marganiec [d], T. Martínez [f], C. Massimi [y], P.F. Mastinu [q], M. Mastromarco [e], M. Meaze [e], E. Mendoza [f], A. Mengoni [z], P.M. Milazzo [aa], F. Mingrone [y], M. Mirea [ab], W. Mondalaers [ac], A. Pavlik [x], J. Perkowski [d], A. Plompen [ac], J. Praena [n], J.M. Quesada [n], T. Rauscher [ad], R. Reifarth [c], A. Riego [l], F. Roman [i,ab], C. Rubbia [i,ae], R. Sarmento [m], P. Schillebeeckx [ac], S. Schmidt [c], G. Tagliente [e], J.L. Tain [p], A. Tsinganis [i], S. Valenta [g], G. Vannini [y], V. Variale [e], P. Vaz [m], A. Ventura [z], R. Versaci [i], M.J. Vermeulen [u], V. Vlachoudis [i], R. Vlastou [o], A. Wallner [x], T. Ware [j], M. Weigand [c], C. Weiß [t], T.J. Wright [j], P. Žugec [k]

[a] Universidade de Santiago de Compostela, Spain
[b] Centre National de la Recherche Scientifique/IN2P3 -Université Paris-Sud - IPN, Orsay, France
[c] Johann-Wolfgang-Goethe Universität, Frankfurt, Germany
[d] Uniwersytet Łódzki, Lodz, Poland
[e] Istituto Nazionale di Fisica Nucleare, Bari, Italy
[f] Centro de Investigaciones Energeticas Medioambientales y Tecnológicas (CIEMAT), Madrid, Spain
[g] Charles University, Prague, Czech Republic
[h] Commissariat à l'Énergie Atomique (CEA) Saclay - Irfu, Gif-sur-Yvette, France
[i] European Organization for Nuclear Research (CERN), Geneva, Switzerland
[j] University of Manchester, Oxford Road, Manchester, UK
[k] Department of Physics, Faculty of Science, University of Zagreb, Croatia
[l] Universitat Politecnica de Catalunya, Barcelona, Spain
[m] Instituto Tecnológico e Nuclear, Instituto Superior Técnico, Universidade Técnica de Lisboa, Lisboa, Portugal
[n] Universidad de Sevilla, Spain
[o] National Technical University of Athens (NTUA), Greece
[p] Instituto de Física Corpuscular, CSIC-Universidad de Valencia, Spain
[q] Istituto Nazionale di Fisica Nucleare, Laboratori Nazionali di Legnaro, Italy
[r] Aristotle University of Thessaloniki, Thessaloniki, Greece
[s] Bhabha Atomic Research Centre (BARC), Mumbai, India
[t] Atominstitut, Technische Universität Wien, Austria
[u] University of York, Heslington, York, UK
[v] Karlsruhe Institute of Technology, Campus Nord, Institut für Kernphysik, Karlsruhe, Germany
[w] Oak Ridge National Laboratory (ORNL), Oak Ridge, TN 37831, USA
[x] University of Vienna, Faculty of Physics, Austria
[y] Dipartimento di Fisica, Università di Bologna, and Sezione INFN di Bologna, Italy
[z] Agenzia nazionale per le nuove tecnologie, l'energia e lo sviluppo economico sostenibile (ENEA), Bologna, Italy
[aa] Istituto Nazionale di Fisica Nucleare, Trieste, Italy
[ab] Horia Hulubei National Institute of Physics and Nuclear Engineering - IFIN HH, Bucharest - Magurele, Romania
[ac] European Commission JRC, Institute for Reference Materials and Measurements, Retieseweg 111, B-2440 Geel, Belgium
[ad] Department of Physics and Astronomy - University of Basel, Basel, Switzerland
[ae] Laboratori Nazionali del Gran Sasso dell'INFN, Assergi (AQ), Italy

* Corresponding author. Present address: Department of Physics and Astronomy, Uppsala University, P.O. Box 516, 751 20 Uppsala, Sweden.

http://dx.doi.org/10.1016/j.nima.2013.12.056
0168-9002/

ARTICLE INFO

Article history:
Received 7 October 2013
Received in revised form
5 December 2013
Accepted 30 December 2013
Available online 8 January 2014

Keywords:
Fission
Neutron
Anisotropy
Angular distribution
^{232}Th
Gas detectors

ABSTRACT

A fission reaction chamber based on Parallel Plate Avalanche Counters (PPACs) was built for measuring angular distributions of fragments emitted in neutron-induced fission of actinides at the neutron beam available at the Neutron Time-Of-Flight (n_TOF) facility at CERN. The detectors and the samples were tilted 45° with respect to the neutron beam direction to cover all the possible values of the emission angle of the fission fragments. The main features of this setup are discussed and results on the fission fragment angular distribution are provided for the ^{232}Th(n,f) reaction around the fission threshold. The results are compared with the available data in the literature, demonstrating the good capabilities of this setup.

1. Introduction

Accurate data on neutron-induced fission cross-sections at intermediate energies are crucial for different fields in physics. In particular, thorough knowledge of the reactions involved in the so-called thorium cycle is important to improving the existing nuclear energy-related technologies.

An extensive experimental program [1] is being carried out at the Neutron Time-Of-Flight (n_TOF) facility at CERN in order to provide accurate values of the cross-sections of neutron-induced reactions, with particular reference to fission and radiative capture.

The fission fragment angular distribution (FFAD) is an important observable for understanding the fission mechanism; especially for studying the quantum properties of the levels of fissioning nuclei for a given J and K (total spin and its projection on the nuclear symmetry axis) when considering energies close to the thresholds of the different multiple-chance fission channels [2]. This makes it possible to describe the existence of a vibrational structure around the fission threshold for the light isotopes of Th, Pa and U [3]. Simultaneous reproduction of fission cross-section and fragment angular distribution is important for the determination of the best set of fission barrier parameters [4].

The anisotropy of the angular distribution of the fission fragments at high energies is also a controversial question. Some theoretical models indicate that fission above several tens of MeV should be isotropic and equal for both proton- and neutron-induced fission. However, a non-isotropic behavior was found for fission of ^{232}Th and ^{238}U with neutrons up to 100 MeV [5]. Therefore, new measurements of the angular distribution of fission fragments are needed to clarify this situation, and the n_TOF facility, with a neutron beam covering an energy range from thermal up to GeV, can supply new data with high accuracy.

Apart from the theoretical implications, the strong anisotropies observed at the thresholds of different chances of neutron emission before fission also affect the fission cross-section measurements due to the angular limitation of the detectors. One of the experimental setups used at CERN n_TOF for studying the fission process is a reaction chamber containing Parallel Plate Avalanche Counters (PPACs). During the Phase1 of the n_TOF project (2001–2004), the fission cross-sections of several nuclei were measured [6,7]. However, due to the limited angular acceptance exhibited by these detectors, only emission angles below $\sim 60^\circ$ were detectable, thus requiring a correction for fragments stopped in the material layers. These corrections were largely determined by the angular distribution of the emitted fragments, for which only incomplete data were available in the literature.

Therefore, a new setup based on a modified geometrical configuration was developed to overcome this difficulty and to obtain full coverage of the angular distribution of the emitted fragments. It was first used during the 2010 and 2011 campaigns (n_TOF-Phase2) to measure ^{232}Th(n,f) [8], following the procedure described in the present work.

E-mail address: dtarriov@gmail.com (D. Tarrío).

2. Experimental setup

The experiment was performed at the CERN n_TOF facility, where a very intense neutron flux is produced by spallation reactions on a lead target using the 20 GeV/c proton beam from the Proton Synchrotron at CERN. The water surrounding the spallation target acts as a moderator to produce a neutron flux covering a wide neutron energy range, from thermal up to more than 1 GeV. The long (185 m) flight path between the spallation target and the experimental area makes it possible to perform high-resolution time-of-flight (TOF) measurements. A detailed description of the facility can be found in Ref. [9].

2.1. Parallel Plate Avalanche Counter

The PPACs used in this experiment have a central anode flanked by two cathodes. A low-pressure gas fills the 3.2 mm gaps between 1.7 μm aluminium coated Mylar foils, which act as electrodes. PPAC anode signals are very fast (9 ns FWHM), reducing the pile-up probabilities and making it possible to reach energies as high as 1 GeV, since these detectors are quite insensitive to the γ-flash created by high energy reactions at the spallation target [9].

The cathodes of each PPAC are segmented in 100 strips 1.9-mm wide and with a separation of 100 μm. The strips on the cathodes are arranged perpendicular to each other, so that the trajectory of the fission fragments (FF), and therefore their angular distribution, can be reconstructed. The anode is connected to a high voltage of around 540 V, while the cathodes are grounded.

The fission reaction chamber includes 10 PPACs with 9 samples in between, and fission events were identified by coincident anode signals of two consecutive PPACs. The chamber was operated with a forced flow of C_3F_8 at a constant pressure of 4 mbar.

2.2. Geometrical configurations

The main difference between the Phase1 and Phase2 setups is their geometrical configuration: in Phase2 the detectors and the samples were tilted 45° with respect to the neutron beam direction, as shown in Fig. 1. This modification was introduced to increase the range of the accessible $\cos\theta$ values, and it was used in the 2010, 2011 and 2012 campaigns to measure the angular distribution of emitted fragments in fission.

2.3. Samples

In the experiment described here, six samples of ^{232}Th, one sample of ^{237}Np, and reference samples of ^{235}U and ^{238}U were used (Fig. 1). The 8 cm diameter samples were built at the IPN-Orsay (France), and were produced by molecular plating of the oxides ThO_2 and UO_3 on an aluminium foil. This foil was 2.5 μm thick in the cases of ^{235}U, ^{238}U and ^{237}Np, and 0.7 μm for the ^{232}Th samples. The mass distributions, total masses, and chemical compositions of the uranium samples were determined by Rutherford Backscattering Spectroscopy (RBS). The ^{235}U and ^{238}U masses were also measured independently by α spectroscopy. Isotopic impurities of ^{238}U (6.28% in number of atoms), ^{234}U (0.74%), and ^{236}U (0.27%) were found in the ^{235}U sample, being negligible the contaminants in the other samples.

3. Simulations

The angular acceptance and the total detection efficiency of the new experimental setup, as well as of the former setup (where the detectors and the targets were perpendicular to the beam direction) have been investigated by simulations with the Geant4 software package [10].

3.1. The simulation setup

A simplified version of the real setup was implemented in the Geant4 simulation, consisting of only two PPACs and one ^{235}U sample in between. The detection efficiency was limited by the stopping power of the different layers that the fission fragments had to traverse, thus only the material layers of the sample and of the active part of the detector were included in the simulation: the gas, the detector electrodes, the sample backing and the sample itself.

Each simulated PPAC detector consisted of three thin layers: one for the central anode and two for the cathodes on either side of it. All electrodes were simulated using Mylar foils of 20×20 cm^2 and 1.7 μm−thick, separated by a 3.2 mm gas gap.

The simulated sample was a 8 cm diameter disc of 15 mg of ^{235}U deposited in the form of $UO_3(H_2O)_5$. It has been found that the uranium oxide UO_3 is hygroscopic and so a certain number of water molecules must be added to the target description to calculate the detection efficiency. In order to show the characteristics of the detection efficiency capabilities of the detection setup, aluminium backings with thicknesses of 0.7 μm and 2.5 μm have been simulated.

The distance between the sample and the detectors was 25 mm. All the elements were surrounded by C_3F_8 gas at 4 mbar, as in real experiments.

To optimize the geometrical configuration, the simulation code was written in such a way that the tilting angle of the samples and the detectors can be set to any desired value with respect to the beam direction.

3.2. Fission event generator

In order to implement a fission generator for the simulation, we have not considered the reaction between the neutron and the nucleus, but directly the fission products. Therefore, in each simulated event, two complementary fission fragments are emitted in opposite directions from a random position inside the sample volume. In general, the fission fragment characteristics (charge, mass, kinetic energy and emission angle) of each simulated event depend on the sample material and the neutron energy, and are selected by a fission event generator specifically created for this purpose.

To obtain the mass and the charge of the emitted fragments we can use the fission yields provided by evaluations. In the present work, we have used the evaluated data for ^{235}U(n,f) with thermal neutrons available in the ENDF/B-VII.1 library [11] to weigh the selection of complementary pairs of fission fragments.

To simulate a fission event, a first fission fragment is randomly selected according to a probability distribution given by the evaluated fission yield. The complementary fission fragment is chosen to get the total amount of protons and neutrons of the fissioning nucleus, from which a random number of neutrons ν were previously removed. The value of ν is given by a Gaussian probability distribution centred at the emission of 2 neutrons and with $\sigma = 1.5$ neutrons.

The fragment kinetic energy is calculated by using the total kinetic energy (TKE) released in the fission, given by Viola's systematics [12]:

$$TKE = 0.1189 \cdot Z^2/A^{1/3} + 7.3 \text{ MeV} \quad (1)$$

Because of the linear momentum conservation, the kinetic energy is distributed between both fission fragments according to the inverse relation of their masses. Due to neutron evaporation, the energy of the FF is reduced according to the number ν of emitted neutrons by a factor $(A-\nu)/A$.

Finally, fission fragments are emitted with an angular distribution that depends on both the nucleus and the neutron energy [2,13–15] but, in the case of ^{235}U at energies below 1 keV, the angular distribution is isotropic and becomes a reference for the characterization of the angular dependence of the efficiency.

3.3. Simulation of the detection efficiency

Assuming a 100% detection efficiency of PPACs for fission fragments [16], events are considered *detected* when both fission fragments pass through the active gas gaps of the PPACs.

When the PPACs and the sample are perpendicular to the neutron beam direction, the distance travelled by a fission fragment inside the material layers is proportional to $1/\cos\theta$, being θ defined as in Fig. 2. Therefore, energy loss is minimal for those fission fragments crossing the detectors in the direction of the beam ($\cos\theta = 1$) and increases with $1/\cos\theta$ until one of the fission fragments (FF) is completely stopped. It is worth to mention, however, that this maximum angle is dependent on the backing thickness. Simulations indicate that the efficiency drops at angles around $\theta = 66°$ ($\cos\theta = 0.4$) for the thin aluminium backing (0.7 μm thick), and at $\theta = 57°$ ($\cos\theta = 0.55$) for the thick one (2.5 μm thick) being, in both cases, more constraining than the geometrical acceptance, that extends up

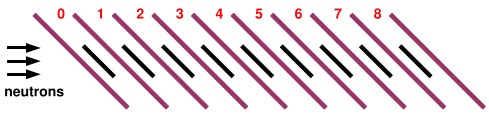

Fig. 1. Schematic top view of the PPAC detectors and the targets used during n_TOF-Phase2. The samples were ^{235}U (target with number 0 in figure), ^{238}U (target 1), ^{237}Np (target 3) and ^{232}Th (targets 2, and from 4 to 8).

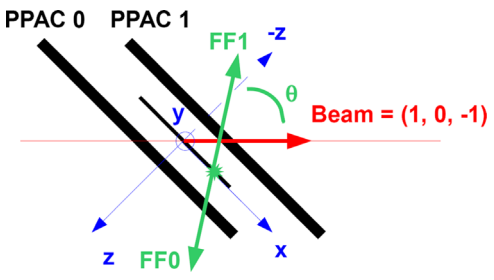

Fig. 2. Reference system used to calculate the emission angle θ of the fission fragments.

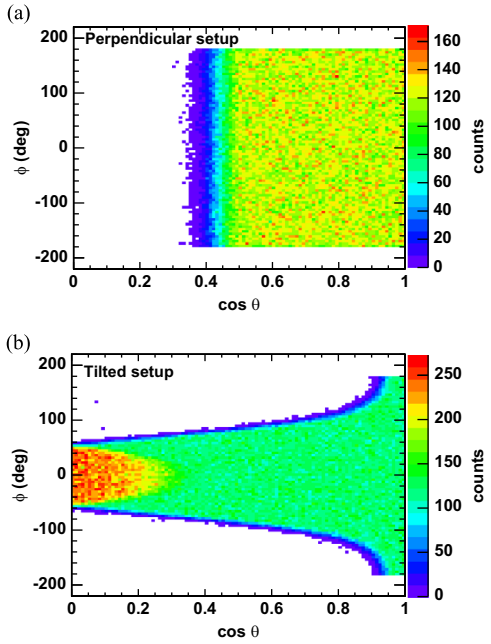

Fig. 3. Simulation of detected events as a function of ϕ and $\cos\theta$ for both geometrical setups: in the perpendicular configuration (a), $\cos\theta$ is limited to angles below 65° and it does not depend on the azimuthal angle ϕ around the beam axis; in the tilted setup (b) all the possible values of $\cos\theta$ between 0 and 1 are covered, and there is a dependence on the azimuthal angle ϕ. See the text for more details.

to $\theta = 77°$ ($\cos\theta = 0.22$). Fig. 3(a) represents the relation between $\cos\theta$ and the azimuthal angle ϕ around the beam axis for detected events (using the 0.7 μm thick backing). In this case, there is no dependence on the ϕ angle around the beam axis.

For the tilted setup represented schematically in Fig. 2, the angular range includes all the values of $\cos\theta$ between 0 and 1 and the efficiency depends on both angles θ and ϕ, as it can be seen in Fig. 3(b) for the detected events. The accumulation of events at low $\cos\theta$ values corresponds to those events where the forward PPAC detects the backward fragment because of the tilt angle.

The detection efficiency is shown in Fig. 4 (using the 0.7 μm thick backing) as a function of $\cos\theta$ for different values of the angle α between the neutron beam axis and the normal to the detector surface. In the perpendicular setup ($\alpha = 0°$), the efficiency was very close to 1 for $\cos\theta \geq 0.5$ ($\theta \leq 60°$) dropping to zero for larger angles. It can be seen from this figure that for tilting angles above $\alpha = 20°$ the efficiency presents a non-zero value from $\cos\theta = 0$ to $\cos\theta = 1$, showing, however, a shoulder around $\cos\theta = 0.7$–0.8. This shoulder-shape is sensitive to the precise definition of the sample thickness. Therefore, when comparing data from two samples a correction factor must be applied to take into account the differences in the detection efficiency, as it will be explained later.

Despite the different behavior of the angular acceptance as a function of the tilt angle α, the overall detection efficiency is nearly the same up to $\alpha = 45°$ (from 0.584 ± 0.003 to 0.572 ± 0.003, see the inset in Fig. 4). For the configuration with $\alpha = 65°$ the efficiency is flatter but this is at the expense of the global efficiency which drops till 0.457 ± 0.003. Therefore, $\alpha = 45°$ is a good compromise between full angular coverage ($0° \leq \theta \leq 90°$) and global efficiency.

3.4. Linear momentum transfer

For neutrons above several MeV, the nucleus acquires a linear momentum that is not negligible, but smaller than the complete

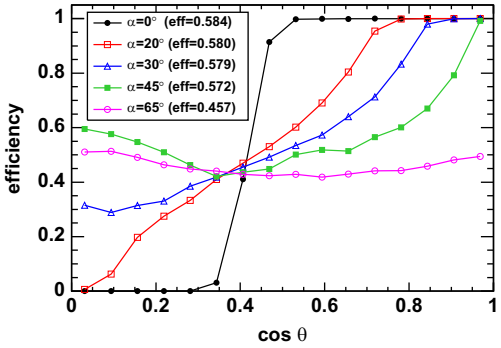

Fig. 4. Simulated detection efficiency for different values of the α angle between the normal to the detectors and the neutron beam direction. The total detection efficiency for each case is indicated in the legend, with a statistical uncertainty of ± 0.003 in all cases.

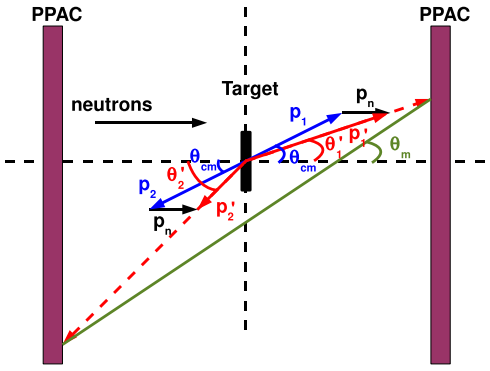

Fig. 5. Kinematics of a fission event detected by two PPACs.

momentum transfer. In the case of proton-induced fission, it reaches a maximum value of ~ 350 MeV/c for proton energies around 1 GeV [17,18]. In order to transform the kinetic energies and the emission angles of the fission fragments from the center-of-mass frame to the laboratory frame, we have used the momentum transfer measured in these experiments of proton-induced fission to assign a value to the momentum transferred by the neutron to the target nucleus.

This transfer of linear momentum implies that the relative angle of emission between both fission fragments is not 180°, contrary to what was assumed in the trajectory reconstruction of fission events. However, in this setup it is not possible to know the emission point of the fission fragments, only their final positions at the PPACs. Therefore, the angle θ_m measured in this setup is different from the emission angle in the laboratory frame. This situation is shown schematically in Fig. 5, where the PPACs are drawn perpendicular to the neutron beam for the sake of simplicity: two fission fragments are emitted in opposite directions in the center-of-mass frame, with momenta p_1 and p_2 at an angle θ_{cm}. The incident neutron transfers a momentum p_n to the nucleus and, therefore, the fragments are emitted with momenta p'_1 and p'_2 at angles θ'_1 and θ'_2 in the laboratory frame, respectively. The measured angle θ_m is determined by the neutron beam direction and by the straight line between the hits in both PPACs.

To study how the linear momentum transferred to the nucleus by the incident neutron affects the emission angle, simulations were done using several typical values of the neutron energy. The relation between the cosine of the emission angle in the CM frame, θ_{cm}, and the cosine of the measured angle θ_m given by the position of the hits in the two PPACs is shown in Fig. 6 for a momentum transfer of 350 MeV/c, which corresponds to the maximum momentum transfer achievable in the n_TOF facility. The linear behavior is clear and a fit to the data yields a slope of 1.000 ± 0.001, indicating the difference between the cosine of the measured and

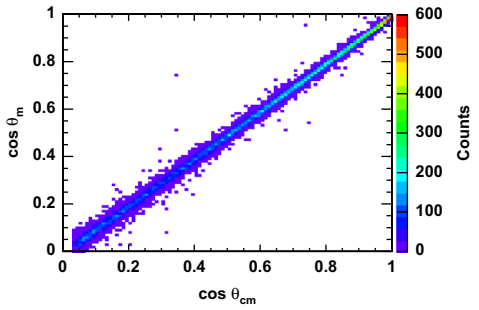

Fig. 6. Relation between the cosine of the measured angle θ_m and the cosine of the emission angle in the center-of-mass frame θ_{cm} as given by the Geant4 simulation for a linear momentum transfer of 350 MeV/c, which corresponds to a 1 GeV neutron.

the cosine of the CM angles to be much smaller than the angular resolution of the experimental setup, which is of 4.5°. Accordingly, the variation introduced by the momentum transfer is negligible, even at the maximum neutron energy of 1 GeV.

4. Data analysis

The PPAC data analysis was based on the coincident detection of both fission fragments in two adjacent PPACs, making it possible to reject most of the background produced by the α activity of the samples and by spallation reactions in the materials surrounding the samples. In this work we followed a similar method to that used in Refs. [6,7] for the identification of fission events using fast anode signals.

To obtain the emission angle, we used the cathode signals that provide the fragment position in each detector. The strips of the cathodes are connected to a delay line that is read from both ends, so that when a signal is produced in a strip, it is conducted to the delay line and is propagated in two directions. The time difference between the ends gives us the spatial position of one coordinate. Since the two cathodes are placed perpendicular to each other, the X and Y positions can be obtained.

In the tilted setup, the reference system used is shown in Fig. 2, where the detectors are parallel to the X–Y plane. The positions of the two fission fragments FF0 and FF1 at both PPACs define a vector $\vec{V}$, while the beam direction is given by the vector $\vec{W} = (1, 0, -1)$. Therefore, cos θ, the variable of physical interest, can be calculated from the dot product of both vectors, assuming that the fragments are emitted with a relative angle of 180°:

$$\cos\theta = \frac{\vec{V}\cdot\vec{W}}{|\vec{V}|\cdot|\vec{W}|} \tag{2}$$

where $|\vec{V}|$ and $|\vec{W}|$ are the magnitudes of $\vec{V}$ and $\vec{W}$, respectively.

For the present work, the neutron energy was measured by the TOF technique using the γ-flash signals for calibration, as described in Refs. [6,7]. This provided a common time reference within 1 ns for all the PPAC detectors and allowed an extremely high energy resolution over the wide energy range of n_TOF.

4.1. Angular distribution measurement

For a certain neutron energy E, the number of detected fission events where the fragments are emitted at an angle θ with respect to the beam direction is given by

$$W(E,\theta)_{detected} = \Phi(E)\cdot N\cdot\frac{d\sigma(E,\theta)}{d\Omega}\cdot\varepsilon(\theta,\phi) \tag{3}$$

where $\Phi(E)$ is the time-integrated neutron fluence (in units of $cm^{-2}\,MeV^{-1}$) for the full measuring time, N is the number of atoms in the target, $d\sigma(E,\theta)/d\Omega$ is the differential cross-section for emission of fission fragments at an angle θ, and $\varepsilon(\theta,\phi)$ is the detection efficiency, which depends on the exit angles θ and ϕ.

To study the angular behavior of the ^{232}Th(n,f) reaction, the dependence of the efficiency factor $\varepsilon(\theta,\phi)$ on cos θ and ϕ introduced in Eq. (3) needs to be subtracted. Since ^{235}U(n,f) is isotropic at low energies, its measured angular distribution directly provides this efficiency factor. As it is shown in Fig. 7, a good agreement between the experimental and the simulated results is obtained for ^{235}U(n,f) below 1 keV. The width of the intervals in the histograms is limited by the statistics we got in this experiment for the six targets of ^{232}Th.

Therefore, the angular distribution functions $W(E,\theta)$ obtained for the ^{232}Th(n,f) were divided by the one measured for ^{235}U below 1 keV. Furthermore, because the backing of the ^{232}Th samples was thinner than the ^{235}U one (as mentioned in Section 2.3), the detection efficiency is not the same in both cases and its ratio has to be taken into account. Therefore, Geant4 simulations have been done to calculate the detection efficiency for the cases where a thick and a thin backing are present, keeping the same ^{235}U deposit as a reference. The ratio of these calculated detection efficiencies is shown in Fig. 8.

Besides the different backing thicknesses, there are small differences between ^{232}Th and ^{235}U samples that can produce variations of the detection efficiency, namely those due to the sample deposition or their amount of water, and even the different energy lost by the fission fragments (different velocities and charges) affecting more as the incidence angle on the different layers is higher. Their relevance has been minimized by selecting only those fission events with an incident angle on the PPACs below 57° (measured with respect to the normal to the detectors). This cut has been applied both to the simulation and the experimental data, being worth to mention that with such a cut the angular acceptance covers all the possible values of cos θ.

The so-obtained FFAD can be parametrized by a sum of even Legendre polynomials $P_L(\cos\theta)$, because of the backward–forward symmetry of the emitted fragments. The least-squares fit of the angular distribution for each neutron energy interval was performed using the following Legendre polynomial series:

$$W(\theta) = C\left[1 + \sum_{L=2L\ even}^{L_{max}} A_L P_L(\cos\theta)\right] \tag{4}$$

where L is the order of the polynomial, L_{max} is the maximum order of the series, and A_L are the fitting coefficients.

Some examples of the angular distributions are shown in Fig. 9, normalized to their values at 90° for easy comparison. The width of the angular intervals was only limited by the available statistics for ^{232}Th. The vertical error bars represent the contribution of the

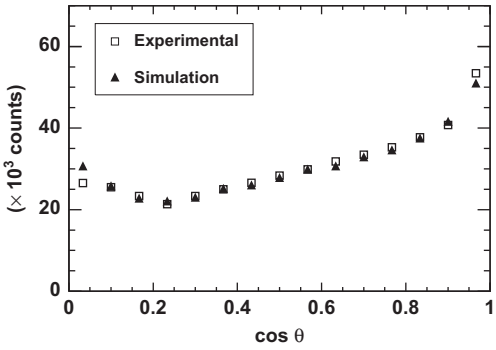

Fig. 7. Experimental cosine distribution of ^{235}U(n,f) for $E_n < 1$ keV, compared with that of the Geant4 simulation. Fission events with an incident angle larger than 57° have been removed (see the text for details). Simulation results, using the thick backing, have been normalized to the experimental data.

statistical uncertainty. Fig. 9(c) and (d) corresponds to a case where the preferred emission was in the beam direction while Fig. 9(a) and (b) shows a side peaked distribution with a minimum at 0°. From the fits shown in Fig. 9(a) and (b) it is evident that the 2nd order polynomial is not enough in all cases, so that Legendre polynomials up to 4th order were used in the fits.

4.2. The anisotropy parameter

The anisotropy parameter is customarily used to characterize the behavior of the angular distribution as a function of the neutron energy, offering us a quick way of comparing our angular distribution results with those available in the literature in the same energy range. It is defined as $A = W(0°)/W(90°)$ and, using Eq. (4), can be written as

$$A = \frac{1 + A_2 + A_4 + \cdots}{1 - \frac{1}{2}A_2 + \frac{3}{8}A_4 + \cdots} \tag{5}$$

that depends only on the coefficients A_2, A_4, … given by the fits to the cosine distributions described in the previous section. This equation works for any L_{max} simply by omitting the unnecessary higher order terms.

In any case, the anisotropy parameter only provides information at 0° and at 90°, while the behavior at intermediate angles remains hidden. For a full description of the angular distribution, it is important to include the values of the fitting coefficients. The results obtained for the anisotropy parameter corresponding to the angular distributions shown in Fig. 9 are related in Table 1 together with the fitting coefficients.

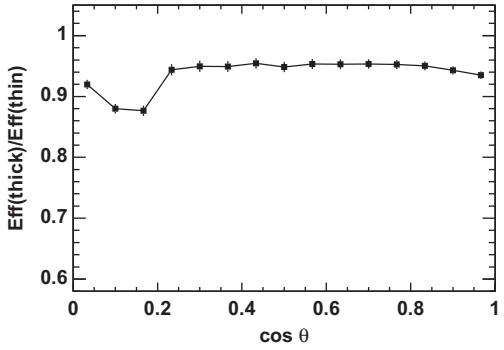

Fig. 8. Simulation result for the ratio of the detection efficiencies for the thin (0.7 μm) and the thick backings (2.5 μm), which correspond to the thicknesses of the backings holding the real samples of ^{232}Th and ^{235}U, respectively. Fission events with an incident angle larger than 57° have been removed (see the text for details).

5. Results

The anisotropy parameter has been calculated by using Eq. (5) for neutron energies between the fission threshold and 3 MeV. Most of the available data cover the region around the fission threshold [15,19–22]. In this range, our data had sufficient statistics to allow for a fine enough energy binning to accurately reproduce the expected behavior. Moreover, because the width of the energy intervals is limited by the counting statistics, the analysis was repeated by using the same number of energy intervals, shifted by the half width of them, giving so a more detailed description of the anisotropy energy dependence. The results from both analysis are represented together in Fig. 10, in which they are compared to existing data. All the results present a maximum of the anisotropy at the fission threshold followed by a deep minimum around 1.6 MeV. This indicates a situation in which

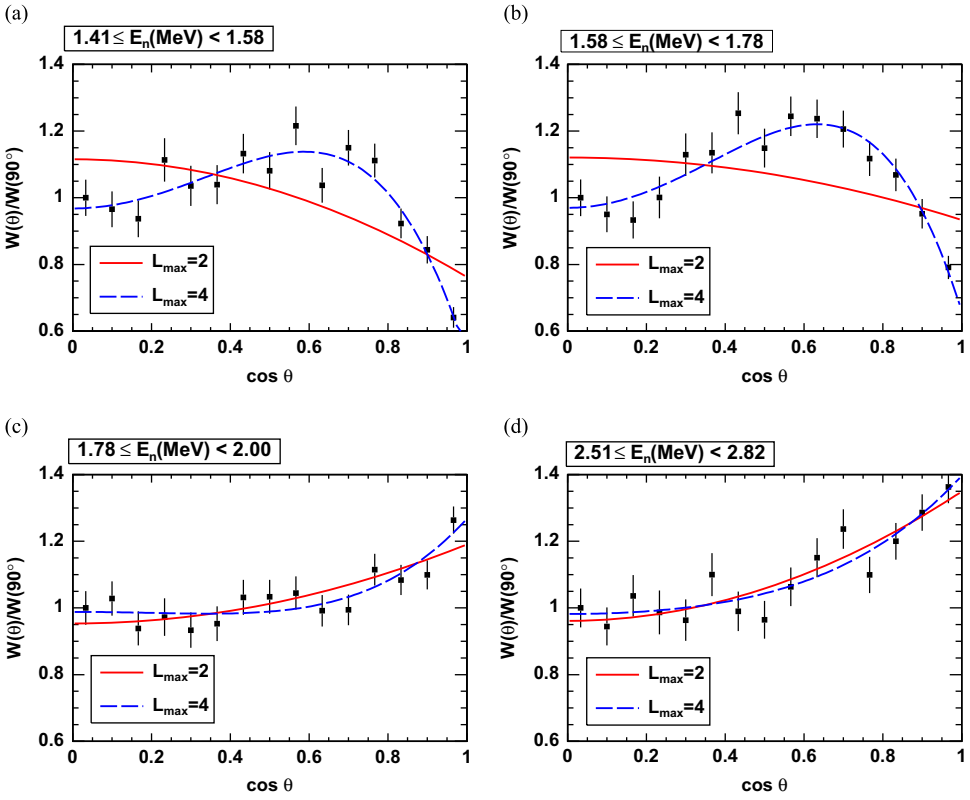

Fig. 9. Examples of angular distributions of fragments emitted in the ^{232}Th(n,f) reaction. In (a) and (b) the angular distribution is side peaked, with a minimum in the beam direction (cos $\theta = 1$), whereas (c) and (d) correspond to a forward peaked distribution, where most of the fragments are emitted along the beam direction. All cases include fits up to the 2nd and the 4th order. The error bars represent the contribution of the statistical uncertainty.

Table 1
Coefficients of the fits to the angular distributions of ^{232}Th(n,f) for the neutron energies shown in Fig. 9 and the values of the anisotropy parameter calculated from them.

E_n (MeV)	A_0	A_2	A_4	$A=\frac{W(0^\circ)}{W(90^\circ)}$
1.41–1.58	1.01 ± 0.01	-0.16 ± 0.03	-0.32 ± 0.04	0.54 ± 0.05
1.58–1.78	1.07 ± 0.01	-0.05 ± 0.03	-0.33 ± 0.04	0.68 ± 0.05
1.78–2.00	1.03 ± 0.01	0.15 ± 0.03	0.08 ± 0.04	1.28 ± 0.05
2.51–2.82	1.09 ± 0.02	0.23 ± 0.03	0.05 ± 0.04	1.42 ± 0.06

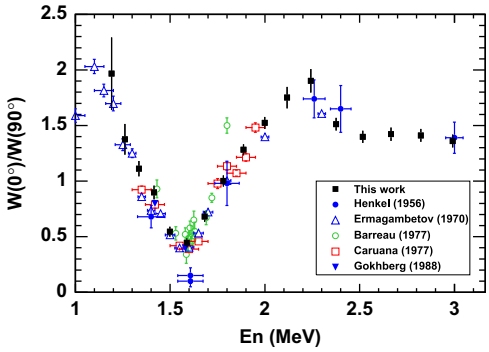

Fig. 10. Dependence of the anisotropy parameter on the neutron energy in the ^{232}Th(n,f) reaction. Present data are indicated by the black squares for comparison with previous results [15,19–22].

the preferred fragment emission changes quickly from forward to sideways direction. At higher energies, only a few measurements are available, showing a broader maximum above 2 MeV.

The accurate reproduction of the anisotropy parameter in this energy range demonstrates the capacity of the tilted setup and of the analysis method to determine angular distributions in a continuous energy range. The use of a wide energy neutron beam, as provided by the n_TOF facility, makes it possible to study the energy dependence with high resolution.

With the position-sensitive PPACs employed in the present work, all possible values of the emission angle could be measured with an uncertainty of $\pm4.5^\circ$. Thus, the full angular distribution was measured and fitted to a Legendre polynomial from which the anisotropy parameter was obtained. This had not been achieved in most of the previous results (Fig. 10), where the measurements were affected by limitations in the angular resolution, imposing limits on the anisotropy parameter calculation. For instance, Henkel and Brolley [15] measured fragments emitted at only five different angles between 0° and 90°, and Caruana et al. [21] at only 6 values. In both works the anisotropy parameter was calculated from fits to Legendre polynomials (up to 6th and 4th order, respectively); Gokhberg et al. [22] calculated the anisotropy parameter as the ratio of the number of fragments emitted in the parallel and perpendicular directions to the beam. In comparison, the present setup is characterized by a continuous angular range with a resolution of $\pm4.5^\circ$, where 15 intervals of $\cos\theta$ were provided for a detailed fit of the angular distributions and for obtaining the respective anisotropy parameters.

6. Summary and conclusions

The performance of a fission chamber based on a new setup of Parallel Plate Avalanche Counters oriented 45° with respect to the neutron beam direction, that was developed for measurements of angular distributions of the fragments from neutron-induced fission, is reported in this paper. The experimental method for measuring the emission angle of the fragments was complemented by Geant4 simulations for calculating the angular-dependent efficiency, being those simulations consistent with the data.

It follows from this study that variations in the target or backing thickness affect the angular dependence of the efficiency. However, it was found that this dependence can be minimized by rejecting those fission fragments hitting the detectors with an incident angle above a certain threshold, which in the present case was set to 57°.

The results obtained for ^{232}Th(n,f) with the continuous neutron beam at the CERN n_TOF facility between fission threshold and 3 MeV have been shown. The good agreement between these results and previous available data proves the capabilities of this setup for providing angular distributions with a good resolution in a neutron beam with a continuous energy distribution. The energy resolution of the results presented here is mainly limited by the counting statistics, whereas the energy resolution of the n_TOF facility is much better (0.5% at $E_n=1$ MeV) [9].

Acknowledgments

We are indebted to Alain Durnez for his precious help in making up the detectors.

This work was partially supported by the Spanish Ministerio de Educación under Grant no. FPU-AP2007-04542, by the Spanish Ministerio de Ciencia e Innovación (MICINN) under Contract nos. FPA2007-62652, FPA2010-22174-C0201, and by the CPAN under Contract CPAN09-PD14.

References

[1] U. Abbondanno, et al., The n_TOF Collaboration, Measurements of Fission Cross Sections for the Isotopes relevant to the Thorium Fuel Cycle, CERN/INTC 2001-025, 2001.
[2] R. Vandenbosch, J.R. Huizenga, Nuclear Fission, Academic Press, New York, 1973.
[3] A.A. Goverdovski, in: Proceedings of the Workshop on Nuclear Reaction Data and Nuclear Reactors: Physics, Design and Safety, Trieste, Italy, 2002.
[4] M. Sin, R. Capote, A. Ventura, et al., Physical Review C 74 (2006) 014608.
[5] I.V. Ryzhov, et al., Nuclear Physics A 760 (2005) 19.
[6] C. Paradela, et al., Physical Review C 82 (2010) 034601.
[7] D. Tarrío, et al., Physical Review C 83 (2011) 044620.
[8] D. Tarrío, Neutron-induced fission fragment angular distribution at CERN n_TOF: the Th-232 case (Ph.D. thesis), Universidade de Santiago de Compostela, Spain, 2012.
[9] C. Guerrero, A. Tsinganis, E. Berthoumieux, The n_TOF Collaboration, European Physical Journal A 49 (2013) 27.
[10] S. Agostinelli, J. Allison, K. Amako, et al., Nuclear Instruments and Methods in Physics Research Section A 506 (2003) 250, Geant4 official webpage: ⟨http://geant4.web.cern.ch/geant4/⟩.
[11] M.B. Chadwick, M. Herman, P. Obložinský, et al., Nuclear Data Sheets 112 (2011) 2887.
[12] V.E. Viola, K. Kwiatkowski, M. Walker, Physical Review C 31 (1985) 1550.
[13] J.E. Brolley, W.C. Dickinson, Physical Review 94 (1954) 640.
[14] J.E. Brolley, W.C. Dickinson, R.L. Henkel, Physical Review 99 (1955) 159.
[15] R.L. Henkel, J.E. Brolley , Physical Review 103 (1956) 1292.
[16] D.N. Poenaru, W. Greiner, Experimental Techniques in Nuclear Physics, Walter de Gruyter, Berlin, 1997.
[17] F. Saint Laurent, M. Conjeaud, R. Dayras, et al., Physics Letters B 110 (1982) 372.
[18] M. Fatyga, K. Kwiatkowski, H.J. Karwowski, et al., Physical Review C 32 (1985) 1496.
[19] S.B. Ermagambetov, G.N. Smirenkin, Soviet Journal of Nuclear Physics 11 (1970) 646.
[20] G. Barreau, C.E.N. Bordeaux-Gradignan Reports 7706, 1977.
[21] J. Caruana, J.W. Boldeman, R.L. Walsh, Nuclear Physics A 285 (1977) 205.
[22] B.M. Gokhberg, L.D. Kozlov, S.K. Lisin, et al., Soviet Journal of Nuclear Physics 47 (1988) 201.